Supplemental Material Table of Contents

Table S1. Oligonucleotides used to target Cas9 mediated KO of *Clcn5*

Guide	Strand	Oligo	Sequence 5'-3'	
G1	(-)	crRNA		AACATGCCACATGTACAAGG
		pHRS	**F:**	AATTATCCCCCTTGTACATG GGCATGTTG
			R:	GATCCAACATGCCACATGTACAAGGGGGAT
G2	(+)	crRNA		GGCCTGAGCTTGGGCAAAGA
		pHRS	**F:**	AATTATGGCCTGAGCTTGGGCAAAGAAGGG
			R:	GATCCCCTTCTTTGCCCAAGCTCAGGCCAT

Table S2. Primer set used to sequence targeted region of *Clcn5* in OK cells

	Sequence 5'-3'
Forward	ATTCTGAGTGGTTTCATCATTCGAG
Reverse	GTGCTCCCTGTGGGAATCTC

Table S3. Primers for qPCR in OK cells

Gene		Sequence 5'-3'
Lrp2	**F:**	AGCCGGACCTGTGTTGATTT
	R:	AAATCAGAGATGCCACGCCA
Cubn	**F:**	AAGAAGGAAAGGTCCTGCATGT
	R:	GTTCAGGAGGGTGACTAGAGC
Gapdh	**F:**	GAGATGCTGGAGCCGAGTA
	R:	GTGGTTCACCCCCATCAC

Table S4. Antibodies for indirect immunofluorescence in OK cells

Primary Antibody Target or Secondary	Company	Catalog #	Source	Working Dilution
Megalin	(Zou et al. 2004)	--	Rabbit	1:1000
Rab11	Abcam	ab65200	Rabbit	1:500
Rab7	Sigma	R8779	Mouse	1:200
EEA1 (E-8)	Santa Cruz	sc-365652	Mouse	1:50
Anti-mouse Alexa Fluor 488	Invitrogen	A11029	Goat	1:500
Anti-rabbit Alexa Fluor 488	Invitrogen	A11034	Goat	1:500
Anti-mouse Alexa Fluor 647	Invitrogen	A21236	Goat	1:500
Anti-mouse Alexa Fluor 647	Invitrogen	A21245	Goat	1:500
F(ab) anti-mouse Alexa Fluor 488	Jackson Immuno	115-547-003	Goat	1:500
F(ab) anti-rabbit Alexa Fluor 488	Jackson Immuno	111-547-003	Goat	1:500
F(ab) anti-mouse (unconjugated)	Jackson Immuno	115-007-003	Goat	1:65
F(ab) anti-rabbit (unconjugated)	Jackson Immuno	111-007-003	Goat	1:65

Table S5. Oligos for generation and characterization of ClC-5 KO mice

		Sequence 5'-3'
Clcn5-E211-guide3		CCAGGGGGCCCTCCTTGCCCGTTTTAGAGCTAGAAATAGCA
Clcn5-E211X-HDR		CCTTGTCATCAAAACTATCACTTTGGTGTTGGCGGTGTCATCTGGCTTGAGCCTGGGC AAATGAATTCCCCTGGTGCACGTGGCTTGCTGCTGTGGGAACATCTTGTGCCACTGCT TCAACAAATACC
Sequencing Primers	**F:**	TGCTGAGGAGTGATAGCGTT
	R:	TGAGTATCCCTAAACACCTGTGG

Table S6. The fractional distribution of cubilin and megalin for WT and ClC-5 KO mice used in the axial model of protein uptake along the PT

WT distribution				**ClC-5 KO distribution**			
	S1	**S2**	**S3**		**S1**	**S2**	**S3**
Cubilin	0.608	0.375	0.018	**Cubilin**	0.699	0.284	0.017
Megalin	0.309	0.646	0.046	**Megalin**	0.400	0.551	0.049

Table S7. Average fractional colocalization (Manders' coefficient) of megalin with endocytic markers for Rescue, ClC-5 KO, and Uncoupled cells

	Rescue			**ClC-5 KO**			**Uncoupled**		
Manders' Coefficient	**Mean**	**SEM**	**N**	**Mean**	**SEM**	**N**	**Mean**	**SEM**	**N**
M_{EEA1}	0.0831	0.0146	23	0.1514	0.0172	27	0.1714	0.0274	22
M_{Rab7}	0.3197	0.0456	25	0.3424	0.0656	25	0.2834	0.0595	25
M_{Rab11}	0.6835	0.0285	20	0.7130	0.0217	20	0.5407	0.0215	15
$M_{LysoTracker}$	0.0296	0.0090	15	0.0223	0.0057	15	0.0589	0.0225	15

Table S8. Average fractional overlap (Manders' coefficient) between endocytic markers for Rescue, ClC-5 KO, and Uncoupled cells.

	Rescue			**ClC-5 KO**			**Uncoupled**		
Manders' Coefficient	**Mean**	**SEM**	**N**	**Mean**	**SEM**	**N**	**Mean**	**SEM**	**N**
$EEA1_{Rab7}$	0.3997	0.0449	15	0.4711	0.0679	15	0.5396	0.0328	15
$EEA1_{Rab11}$	0.2017	0.0269	15	0.0928	0.0250	13	0.1387	0.243	15
$Rab7_{EEA1}$	0.0981	0.0189	15	0.1043	0.0207	15	0.1142	0.0171	15
$Rab7_{Rab11}$	0.0931	0.0294	14	0.0806	0.0208	14	0.1351	0.0316	15
$Rab11_{EEA1}$	0.0367	0.0095	15	0.0045	0.0020	13	0.0228	0.0078	15
$Rab11_{Rab7}$	0.1399	0.0242	14	0.0616	0.0115	14	0.1343	0.0223	15

Table S9. Fractional trafficking kinetics of megalin in Rescue, ClC-5 KO, and Uncoupled cells as percentage of megalin in the originating compartment per minute (mean ± SEM). The synthesis (S) rate and degradation (k_D) rates represent the percent of total megalin synthesized per minute and megalin in M_{lys} that is degraded per minute, respectively.

Rate	Rescue	ClC-5 KO	Uncoupled
k_e	8.31 ± 0.69	8.31 ± 0.69	6.43 ± 0.56
$k_{m,1}$	3.23 ± 0.97	1.72 ± 0.65	1.26 ± 0.49
$k_{DAT,f}$	3.10 ± 0.67	1.65 ± 0.31	1.21 ± 0.26
$k_{DAT,s}$	0.94 ± 0.18	0.86 ± 0.23	0.89 ± 0.24
k_r	0.94 ± 0.12	0.77 ± 0.11	0.94 ± 0.15
$k_{m,2}$	1.10 ± 0.18	1.52 ± 0.37	1.0 ± 0.24
k_d	12.6 ± 4.55	24.5 ± 9.34	5.01 ± 2.19
S	0.31 ± 0.02	0.38 ± 0.03	0.25 ± 0.02

Supplemental Figure Legends

Figure S1. **Impact of ClC-5 KO and Rescue on endocytic uptake of albumin confirmed in multiple clonal lines.** (A) Genomic sequence showing insertion and deletion mutations (red) causing frameshifts predicted to result in early termination of protein translation in ClC-5 KO clones 2-6. The codon encoding the gating glutamate (E225) is shown in blue. (B) Cells from the OK parental population, ClC-5 KO clones 1-6, and Rescue clones 1 and 2 were incubated for 30-60 min with 40 µg/ml Alexa Fluor 647-albumin and then solubilized. Uptake of fluorescent albumin was quantified by spectrofluorimetry as described in Methods and then normalized to the uptake by the OK parental population (n=2-4). Each experiment included a parental OK control but did not always include all of the KO or Rescue clones. Every independent experiment is indicated by a different symbol. Symbols in dark gray are the same data included in Figure 1C.

Figure S2. Expression of megalin and cubilin receptors is coordinately affected by ClC-5 KO. (A) Rescue and ClC-5 KO cells were incubated for 30 min with 100 µg/ml Alexa Fluor 647 albumin on ice and then solubilized. Surface bound albumin was quantified by spectrofluorimetry and normalized to Rescue. ****P<.0001 (n=24) using one-way ANOVA Tukey's multiple comparison test. (B) Rescue and ClC-5 KO cells were incubated with the indicated concentrations of Alexa Fluor 647 albumin at 37°C for 15 min and then rapidly washed and solubilized, and cell-associated albumin was assessed by spectrofluorimetry. (C) Albumin uptake as a function of concentration was modelled and deconvolved into saturable high-affinity and low-affinity uptake components. The high-affinity (V1; left, representing binding to cubilin) and low-affinity (V2; middle, mediated by megalin binding) uptake capacities and the ratio of V2 to V1 (right) calculated for each independent experiment with Rescue and ClC-5 KO cells are plotted as individual points with the mean noted. Note the similar mean V2 to V1 ratio in Rescue and ClC-5 KO cells which indicates that high-affinity and low-affinity uptake components are similarly affected by ClC-5 KO. (D) Equivalent amounts of protein from Rescue and ClC-5 KO cells were blotted for cubilin. The quantified band intensity for each independent experiment was normalized to Rescue cl. *P=0.0182 (n=6) using one-way ANOVA Tukey's multiple comparison test. A representative blot is shown to right. Arrow indicates band at expected molecular weight for cubilin. *Indicates background band.

Figure S3. Quantitation of the overlap between endocytic markers in Rescue and ClC-5 KO cells. Rescue and ClC-5 KO cells cultured on permeable supports were fixed and processed to detect colocalization between the indicated pairs of endocytic compartment markers. Quantification by Manders' coefficient over the entire z-stack for (A) EEA1 and Rab7, (B) EEA1 and Rab11a, and (C) Rab7 and Rab11a is shown as the percent of total. Each point represents a single z-stack image. **P=0.009 (n=13-15) using one-way ANOVA Tukey's multiple comparison test.

Figure S4. Polarity of degraded ^{125}I-albumin excretion is similar in Rescue and ClC-5 KO cells. Rescue and ClC-5 KO cells were incubated with ^{125}I-albumin and chased for 60 min. The apical and basal media were collected, and cells solubilized. Each sample was TCA precipitated to determine how much ^{125}I-albumin was intact versus degraded. The graphs show the average fraction of total internalized ^{125}I-albumin that is degraded or intact in the (A) cell lysate, (B) apical media, and (C) basal media. Each point represents an independent experiment (n=3).

Figure S5. Megalin expression is altered by expression of the uncoupled ClC-5 mutant. (A) Rescue, ClC-5 KO, and Uncoupled cells on permeable supports were fixed and processed to detect actin using

fluorescent phalloidin. Representative maximum projections are shown with single XZ sections shown below. Scale bar: 20 µm. (B) Quantification of the height of the cell monolayer based on actin staining. Each point represents the maximum height of actin staining in a single XZ section (n=28-33 from 3 z-stacks per cell line). (C) Megalin (*Lrp2*) and Cubilin (*Cubn*) transcripts in clones expressing WT ClC-5 or the Uncoupled ClC-5 mutant E211G were determined using quantitative PCR and normalized to *Gapdh* transcript levels. Relative fold change (RFC) of ClC-5 KO cells compared with Rescue cells (normalized to 1; dotted line) is plotted. (D) The apical surfaces of Uncoupled cells was biotinylated, and total (5%) and surface megalin were quantified by blotting. A representative blot is shown above the graph. (E) Rescue, ClC-5 KO, and Uncoupled cells were incubated for 30 min with 100 µg/ml Alexa Fluor 647 albumin on ice and surface bound albumin quantified as described in Methods and normalized to Rescue cells. ****P<0.0001 (n=9-24) using one-way ANOVA Tukey's multiple comparison test. Data for Rescue and ClC-5 are the same as shown in Figure S2A and are plotted in dark gray. (F) Degradation kinetics of apically biotinylated megalin in Uncoupled cells were quantified as described in Methods. Data from 3 independent experiments were used to fit (black line) the degradation rate of megalin using estimates of fractional endocytic rate (Fig. 5D and Table S8) and the fraction of megalin at the apical surface (grey lines: 95% CI). A representative blot showing the decrease in biotinylated megalin over time is shown above the graph. The estimated half-life of surface megalin is shown in the bottom left corner of the graph.

Figure S6. Megalin distribution is altered by the expression of uncoupled ClC-5 mutant. (A-E) Uncoupled cells on permeable supports were fixed and processed to detect colocalization between the indicated pairs of endocytic compartment markers. Quantification by Manders' coefficient over the entire z-stack for (A) megalin with each of the endocytic markers, (B) EEA1 and Rab7, (C) EEA1 and Rab11a, and (D) Rab7 and Rab11a is shown as the percent of total. Each point represents a single z-stack image. **P=0.0073 (n=22) and ***P=0.0007 (n=15) using one-way ANOVA Tukey's multiple comparison test. (E) The average fractional distribution of EEA1 (n=52), Rab7 (n=54), Rab11a (n=45), and megalin (n=76) over the z-axis of a cell, from 0 (apical) to 1 (basal), is plotted. Note the stronger basolateral shift of the megalin distribution of Uncoupled cells compared to ClC-5 KO and Rescue cells (compare to Fig 3F). (F) Representative maximum projections of EEA1 in single cells in Rescue, ClC-5 KO, and Uncoupled cells. Scale bar: 5 µm (G) Quantification of the number and total area of EEA1 spots per cell. Masks were generated from maximum projections of EEA1 staining in cell singles. The number of individual spots and total area in each mask were quantified. This analysis was performed using MATLAB R2021a.

Figure S7. Simulated effect of error in biochemical measurements and assumptions on intracellular trafficking kinetics. (A) The sensitivity of AEE maturation rates ($k_{m,1}$, $k_{,f}$) to error in fraction at the surface ($_S$) measurements for Rescue, ClC-5 KO, Uncoupled cells. $_S$ is plotted relative to the measured values, 6.2%, 5.1%, and 6.7%, respectively (1.0 on x -axis). (B) The sensitivity of AEE maturation rates ($k_{m,1}$, $k_{,}$) to error in endocytic rate (k_L) measurements for Rescue, ClC-5 KO, Uncoupled cells. k_L is plotted relative to the fit values provided in Table S9 (1.0 on x -axis). (C-E) Intracellular trafficking rates (C) $k_{m,1}$, (D) $k_{,}$, (E) and $k_{,L}$, which are dependent on the fraction of megalin recycling through AVs (α) are plotted in response to changes in α for Rescue, ClC-5 KO, and Uncoupled cells. Note that for all values of α the predicted values of $k_{m,1}$ and $k_{,}$ for ClC-5 KO and Uncoupled cells are lower than those for Rescue cells. (F) Schematic of kinetic model of megalin traffic in the PT with trafficking rates denoted.

Figure S8. Sensitivity of megalin internalization to intracellular trafficking kinetics. (A-B) Megalin internalization in ClC-5 KO (A) and Uncoupled (B) cells in response to changes in intracellular trafficking

rates, $k_{m,1}$, $k_{\quad,\quad}$, $k_{\quad,L}$, and k_{L}. Rates are plotted relative to the fit values provided in Table S9 (1.0 on x-axis). The black dotted lines represent the estimated number of megalin molecules internalized per minute in Rescue cells per 10000 molecules of total megalin. Based on blotting data (Fig. 5C), ClC-5 KO and Uncoupled cells have 8,437 and 6,756 total megalin molecules, respectively, when the rate fold-change is 1. Note that changing k_{L} (green line) does not affect megalin internalization. This is due to a reduction in total megalin levels as a consequence of increased cycling through the endocytic pathway. The model predicts a ~30% reduction in total megalin in ClC-5 KO cells when k_{L} is doubled. (C) Schematic of kinetic model of megalin traffic in the PT with trafficking rates denoted.

Figure S9. Calibration curves for chloride concentrations and pH. (A) Cells on filter supports preloaded with BAC- and TMR- dextrans were incubated with ionophores and buffers with indicated [Cl^-] and imaged by confocal microscopy. The ratios of TMR to BAC intensity were measured as described in Methods and fit by linear regression. (B) Representative raw regions of interest (ROIs) of endosomal spots containing internalized BAC- and TMR-dextrans under 0mM or 50mM [Cl-] conditions used in the calibration curve, showing the changes in relative intensities. Scale bar: 1 µm. (C) Cells on filter supports preloaded with FITC- and Alexa Fluor 647-dextrans were incubated with ionophores and buffers with indicated pH and imaged by confocal microscopy. The ratios of FITC to 647 intensity were measured as described in Methods and fit by nonlinear regression with an exponential growth curve. (D) Representative raw ROIs of endosomal spots containing internalized FITC- and 647-dextrans under pH 5.5 or pH 7.5 conditions used in the calibration curve. Scale bar: 1 µm.

Figure S10. **Characterization of ClC-5 KO mice.** (A) Genomic DNA from the founder male was amplified and sequenced in both directions with primers in Table S5. The consensus sequence was blasted against the wild type mouse genome. Upper case text shows shared sequence between WT and ClC-5 KO mice. Forward and reverse primers are indicated in dark blue font. The 189 bp deletion is indicated in lowercase red font. The codon encoding the gating glutamate (E211) is marked by the black box and the vertical black bar indicates the end of exon 6. WT genomic DNA section correlates to nucleotides 7,036,328-7,036,857in GRCm39. (B) Predicted protein sequence of WT and ClC-5 KO mice showing early stop denoted by *. The gating glutamate (E211) in shown in green. Bold font in ClC-5 KO indicates amino acid sequence different from WT. (C) Kidney sections from WT mice (left panel) and ClC-5 KO mice (center, right panels) were stained by H&E. The black box shows a 2X zoom-in of the ClC-5 KO mouse kidney section, highlighting proteinaceous casts (example denoted by the asterisk). (D) Equal volumes of urine collected from WT and CLC-5 KO mice were separated by SDS-PAGE on a stain-free gel to visualize total protein in urine. Note the preferential increase in low molecular weight proteins in ClC-5 KO urine. The intense band at ~20 kDa in both lanes likely represents mouse urinary proteins (MUPs) commonly observed in urine from male mice. (E) Creatinine concentration was determined for each sample. Each symbol represents a different mouse and corresponds to the same mice in Figures 6A, C and 7E, F.

Shipman et al. Figure S1

A

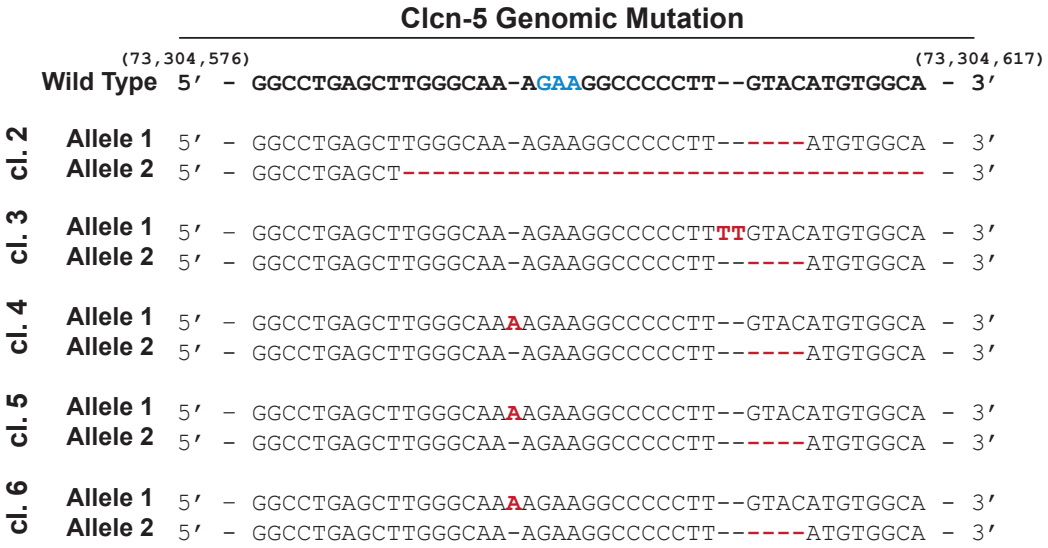

B

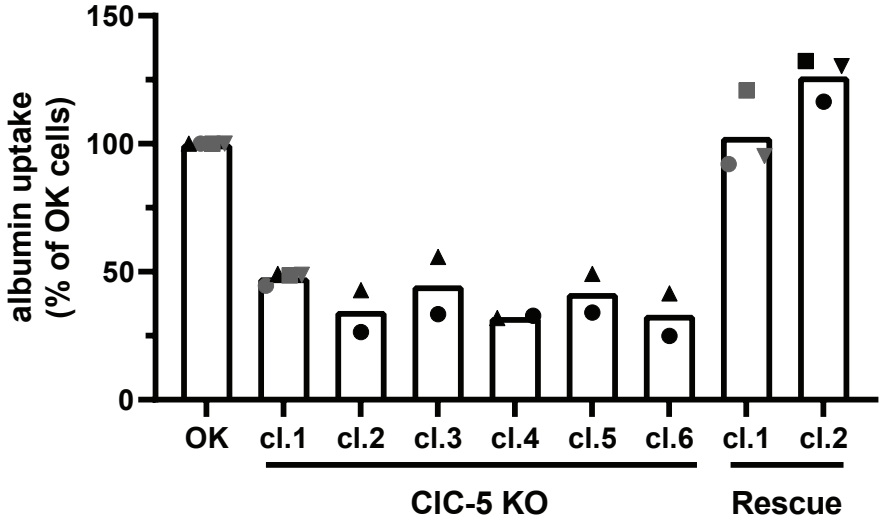

Shipman et al. Figure S2

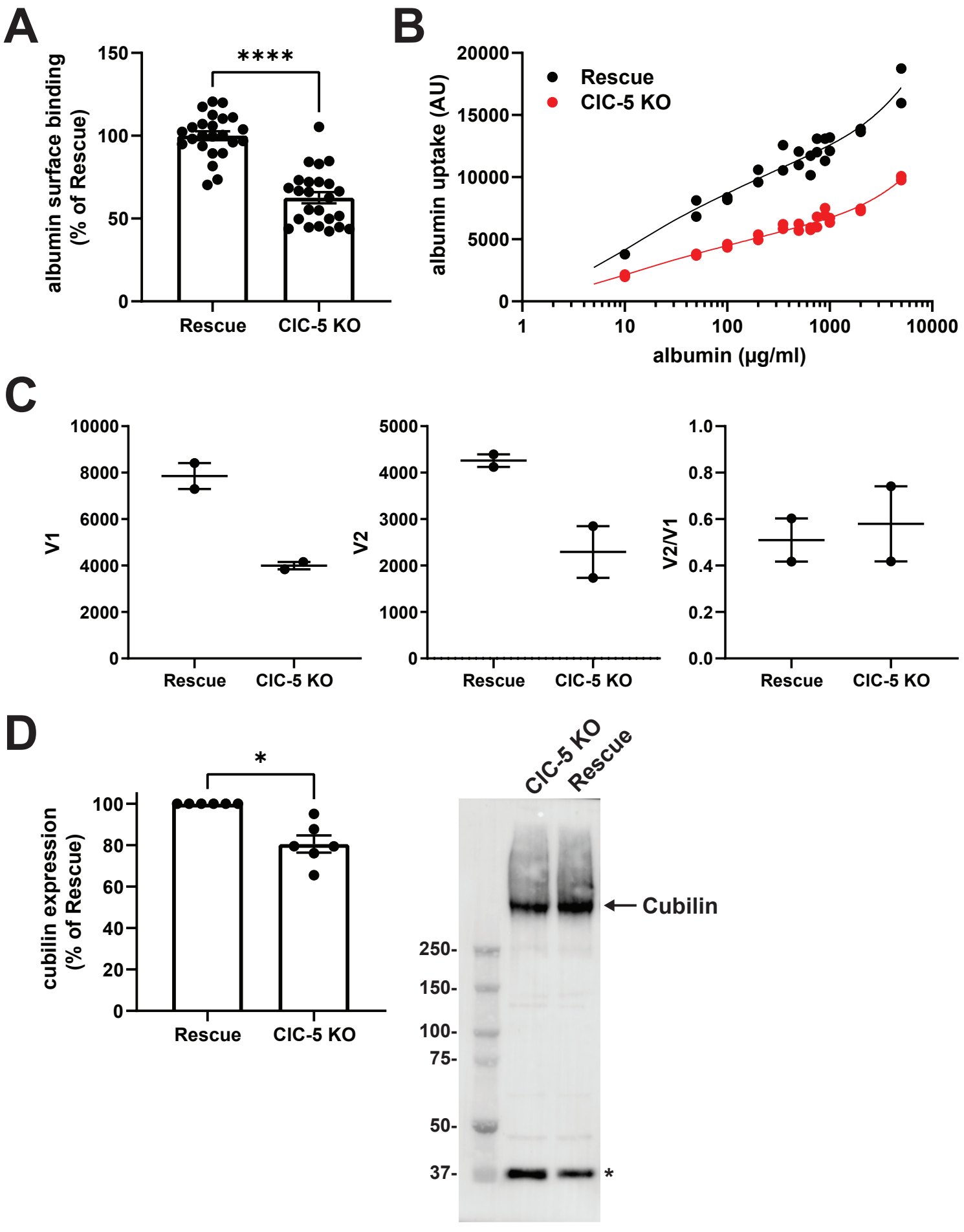

Shipman et al. Figure S3

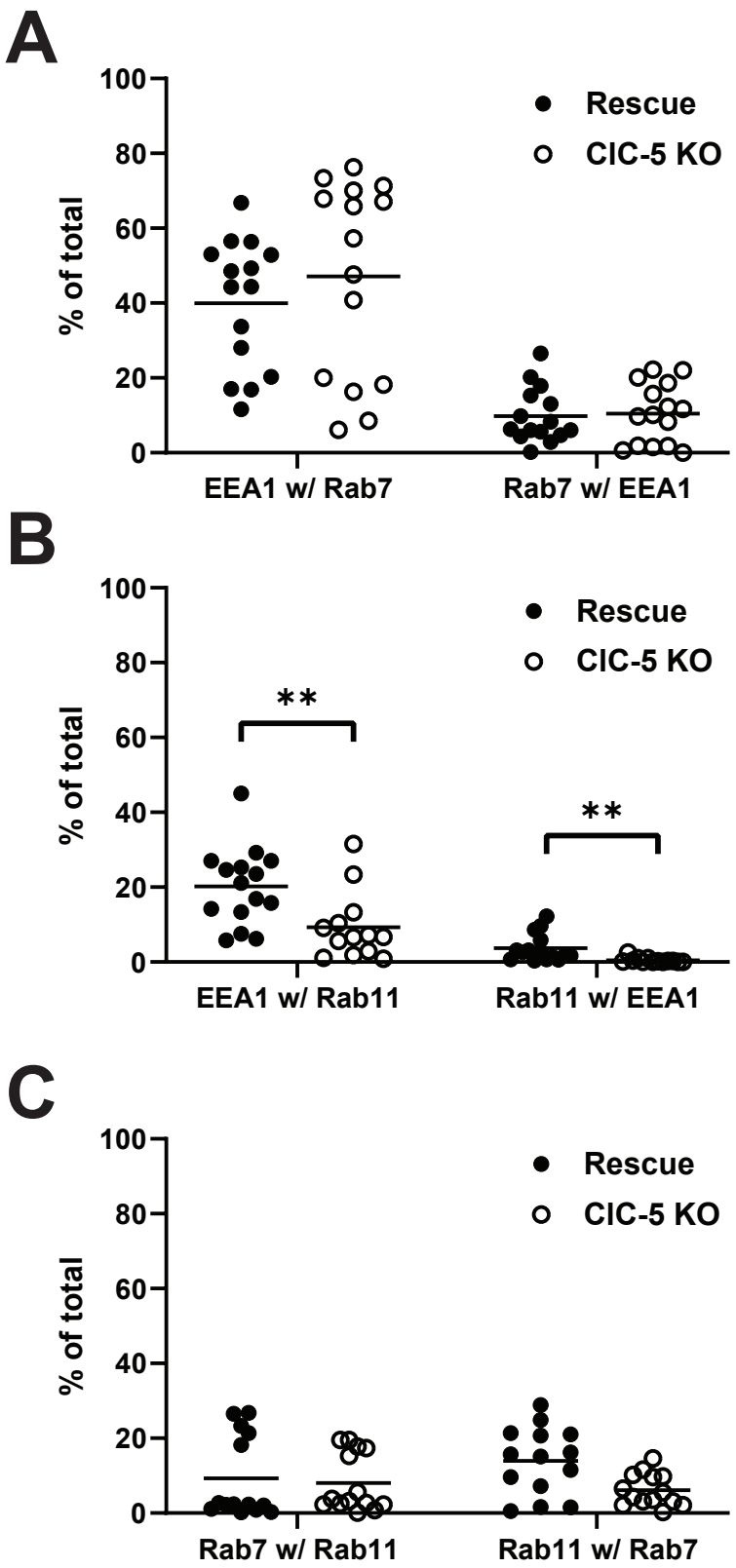

Shipman et al. Figure S4

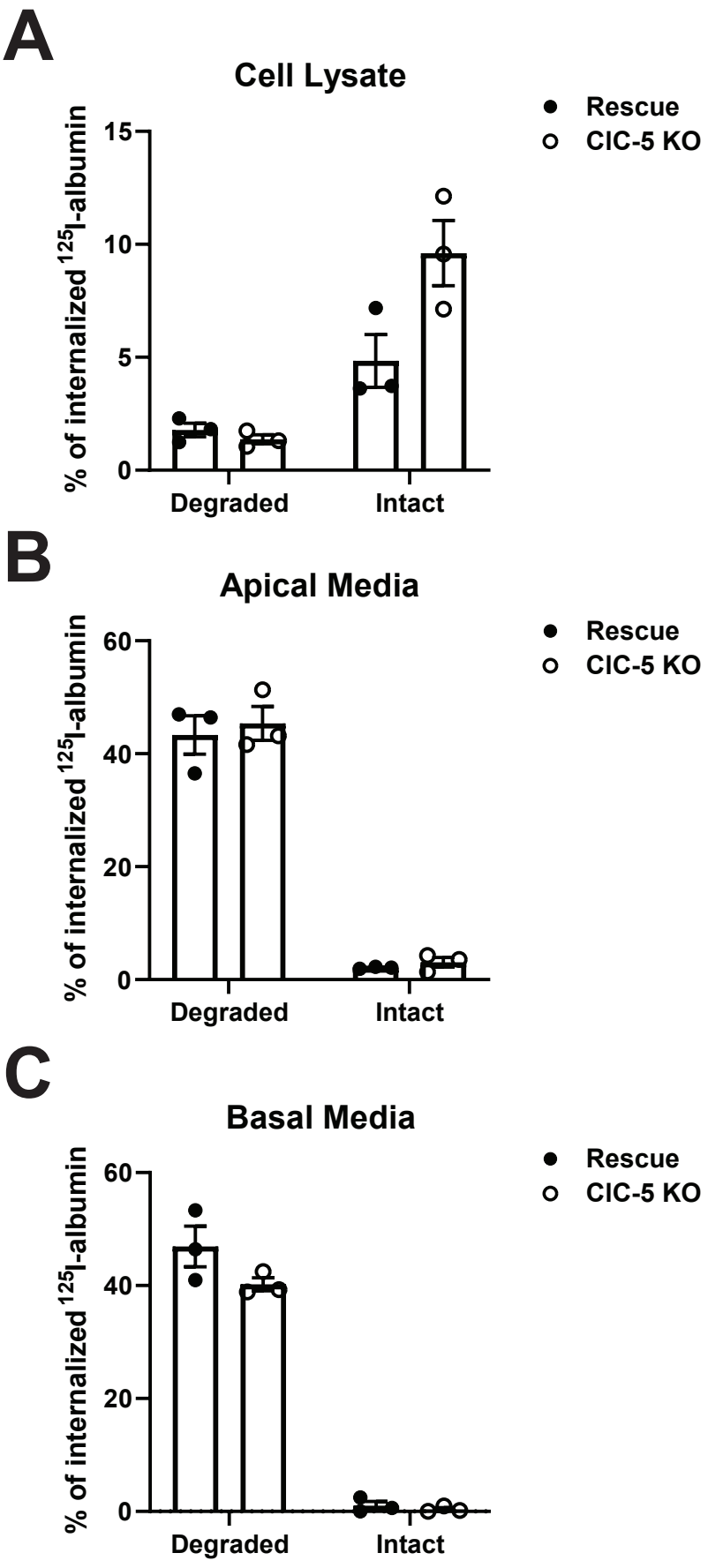

Shipman et al. Figure S5

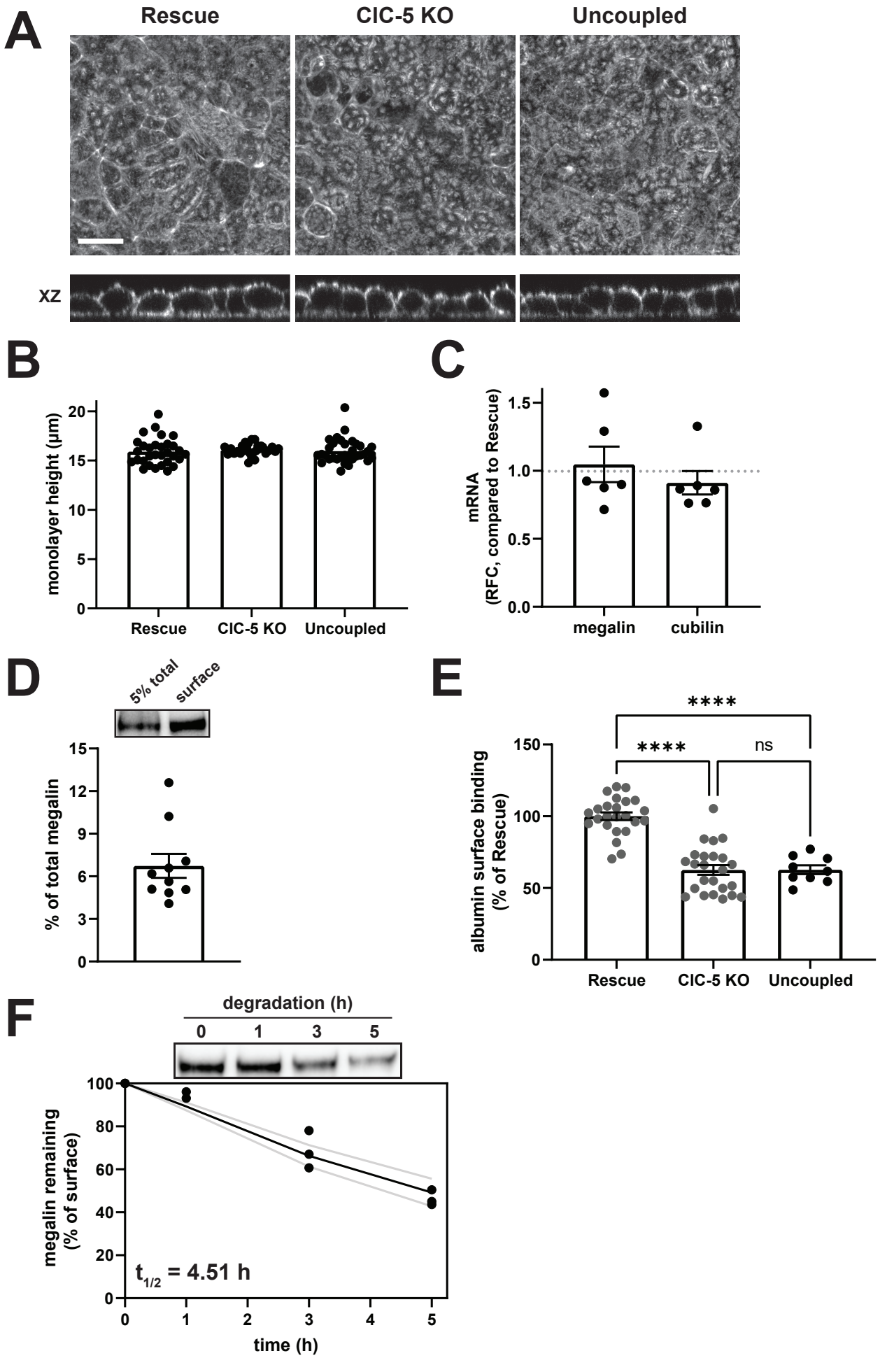

Shipman et al. Figure S6

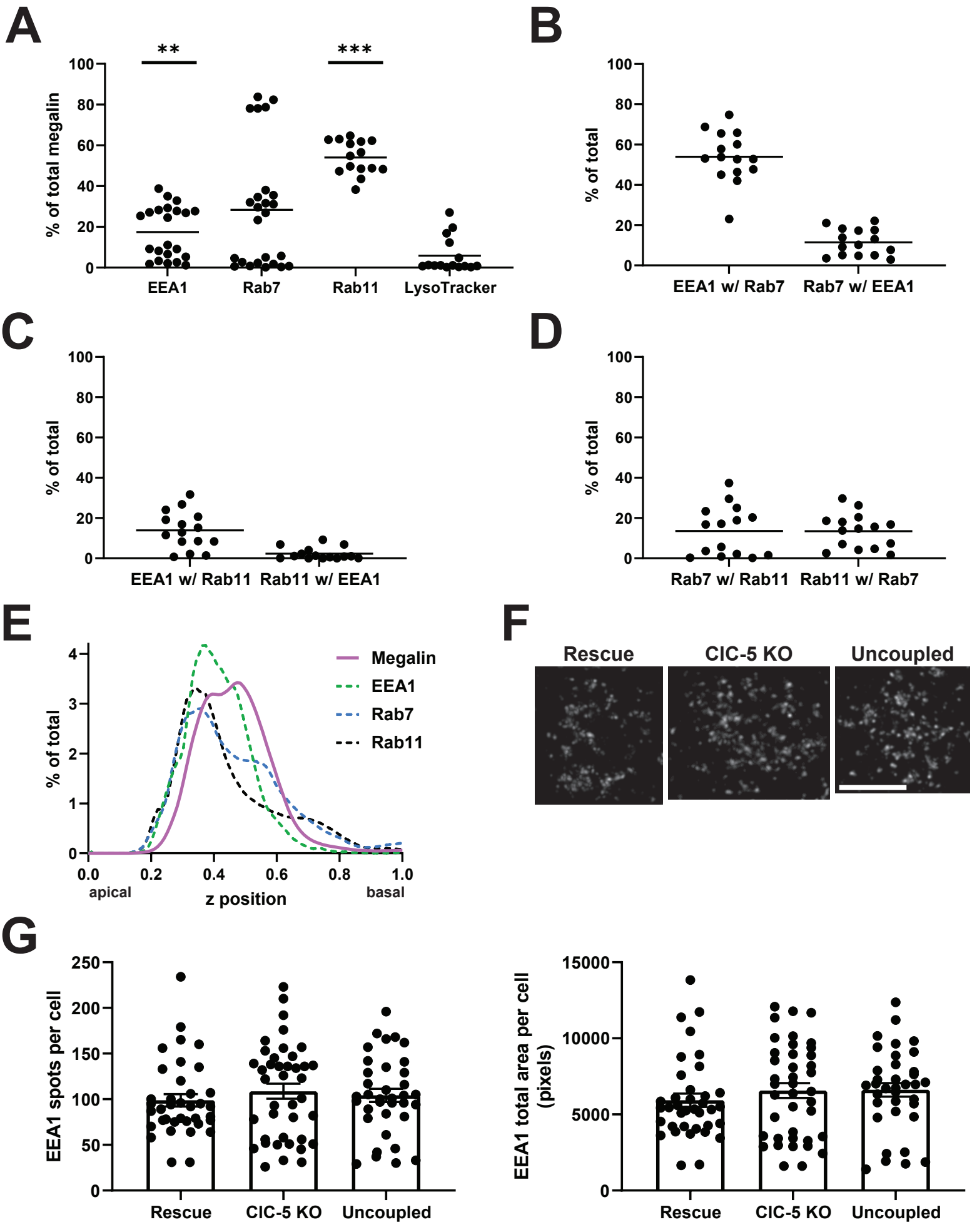

Shipman et al. Figure S7

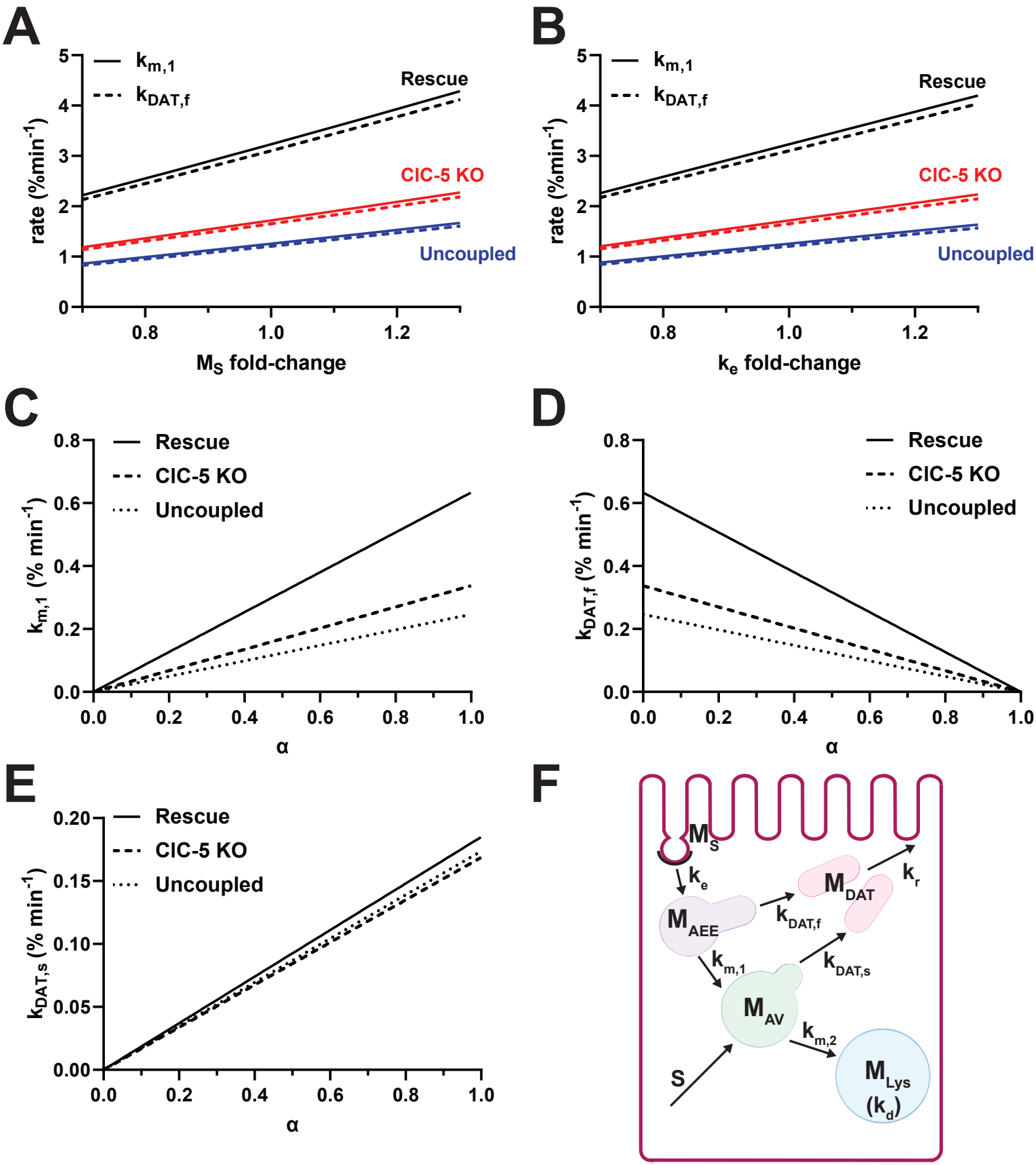

Shipman et al. Figure S8

A

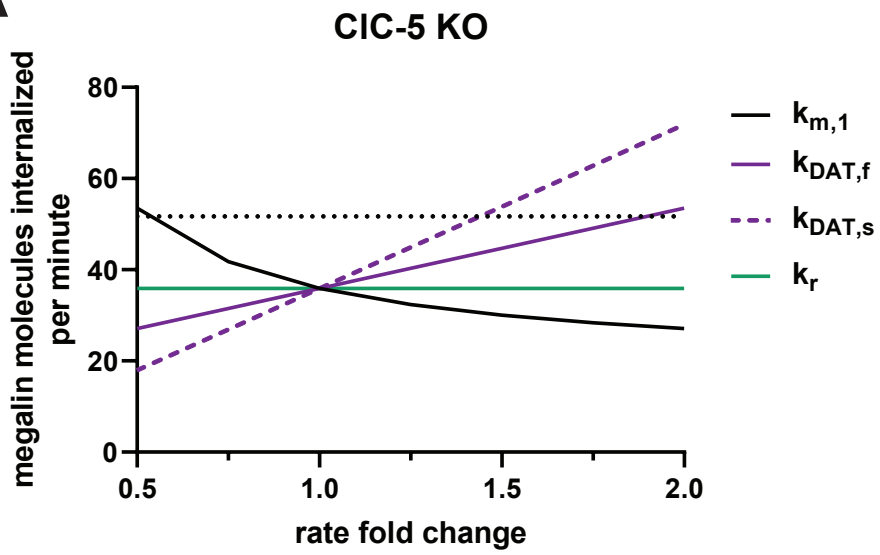

B

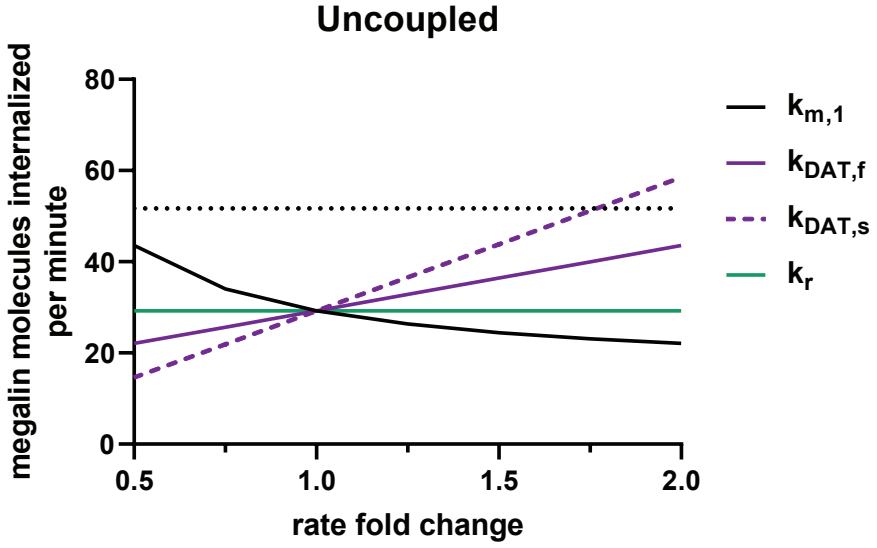

C

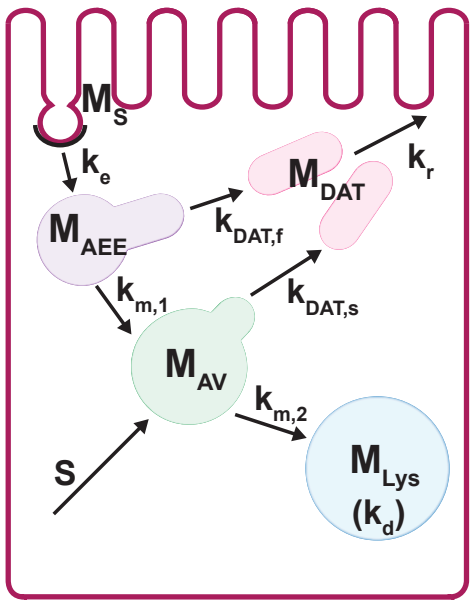

Shipman et al. Figure S9

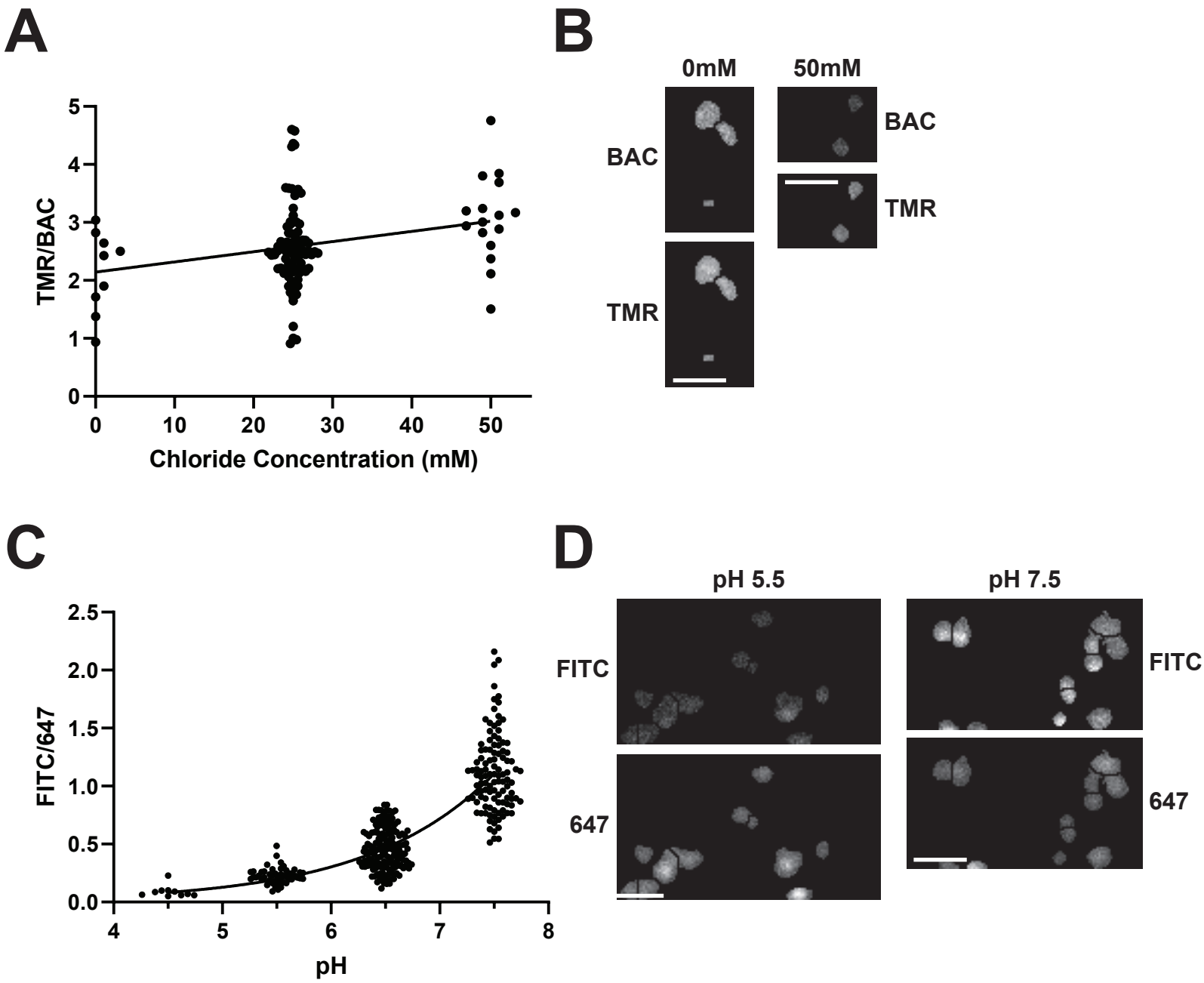

Shipman et al. Figure S10

A

```
TGCTGAGGAG TGATAGCGTT CTTGTGTGGG GTGTAGATTT GAACTGTTTA  7036807
GCCCTGTTTA TTTACGTAGT CTGTTTCCAA TCTCTCTGTG TTTGGCCTGC  7036757
AGATCAAAAC CATCCTGAGT GGTTTCATTA TTAGAGGCTA TCTGGGTAAG  7036707
TGGACCCTTG TCATCAAAAC TATCACTTTG GTGTTGGCGG TGTCATCTGG  7036657
CTTGAGCctg ggcaaggagg gccccctggt gcacgtggct tgctgctgtg  7036607
ggaacatctt gtgccactgc ttcaacaaat accggaagaa tgaagccaag  7036557
cggagagagg taaggacatg tgactttaac agccacccac caccaccttc  7036507
caccctgtgc tctctaaccc cctcaggagc agaagtactg tgctctCAGA  7036457
GATCAAAATT TGGGGATTTC ATGAGGGTAA ATTCAAATAG CTTTTAGTTC  7036407
TGCAGGTTCA GTTCTAGGAG TCCATCTTTT AGCCATCTTA GCATGTGTTT  7036357
ATATATCCAC AGGTGTTTAG GGATACTCA
```

B

```
                (173)                                                (224)
Wild Type  N'-IKTILSGFIIRGYLGKWTLVIKTITLVLAVSSGLSLGKEGPLVHVACCCGNI-C'
CIC-5 KO   N'-IKTILSGFIIRGYLGKWTLVIKTITLVLAVSSGLSQRSKFGDFMRVNSNSF*-C'
```

C

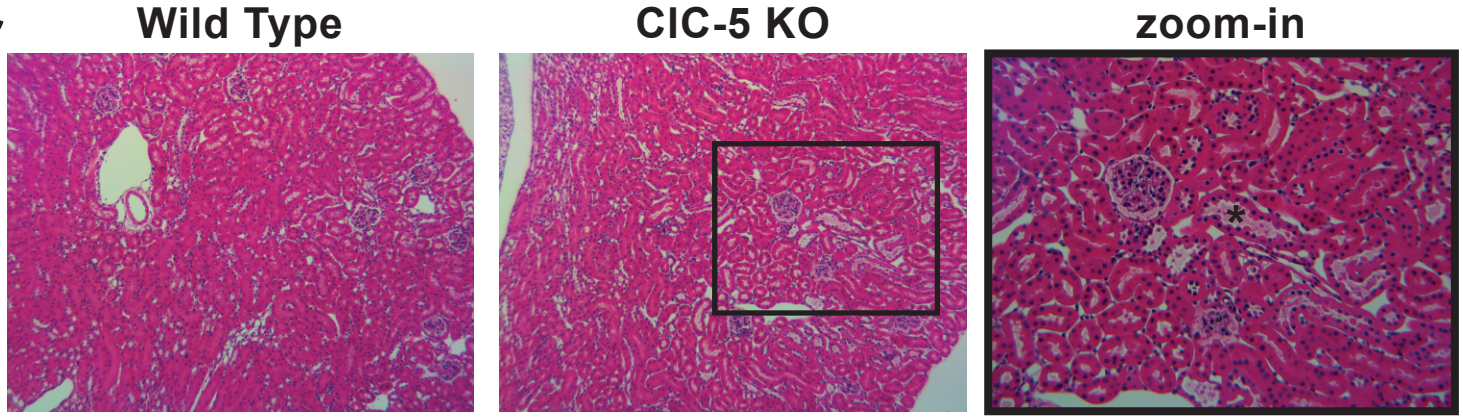

D

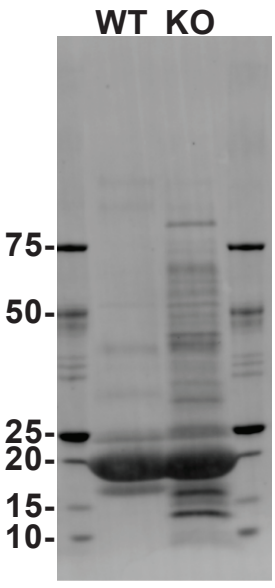

E